THEORETICAL CALCULATION OF HYDROGEN SULFIDE INTERACTION AND ADSORPTION ON SELECTED TiO_2 SURFACE: BY DFT APPROACH

N. NEHAOUA[1,2]*, I. AMI[1,3], F. MEBTOUCHE[1,2], H. MEZIANI[1,2], S.H. ABAIDIA[1,2]

[1] Faculty of Science, Physics Department, University M'Hamad Bougara Boumerdes, 35000, Algeria
[2] Laboratory of Coatings, Materials, and Environment (LRME), M'hamed Bougara Universty of Boumerdes (UMBB), Algeria
[3] Theoretical Physics and Didactics Laboratory, Faculty of Physics, University of Sciences and Technology Houari Boumedien, Algeria
* *E-mail*: n.nehaoua@univ-boumerdes.dz

Received February 15, 2023

Abstract. DFT + U computations were performed to investigate the role of the used approach to study the adsorption and reaction of H_2S on the TiO_2 rutile (110) surface. We present new results using the GGA + PBE approach to clarify the interaction of H_2S molecule with rutile TiO_2 (110) surface, including their structural and electronic properties. Different adsorption configurations were obtained for the initial adsorption sites Ti_{5c}, O_{2c}, and O_{3c} with different H_2S-surface distances. The H_2S preferentially adsorbs dissociatively at the Ti_{5c} site, which is the most energetically favorable site, leaving a dissociated H atom bonded to another O_{2c} site. We have reported the results of the PBE + U calculation including geometrical structure, adsorption energy, electronic density of states, work function, and charge transfer. The inclusion of PBE + D2 interaction increases the adsorption energies. Upon the adsorption process, the calculated work function and band gap are reduced which enhanced the photocatalytic properties of the TiO_2, a stronger adsorption ability indicates a higher capability for H_2S as a detector and sensitive sensors.

Key words: PBE + U, PBE + D2, adsorption, dissociation, Hydrogen sulfide, TiO_2 (110) surface.

1. INTRODUCTION

Titanium dioxide TiO_2 is used in a wide range of technological areas, including photocatalysis, gas sensors, lithium-ion battery anode, and heterogeneous catalyst [1–3] because of its abundance and high stability in different environments. TiO_2 has gained more scientific and industrial attention and attracted much attention as an environmental purification photocatalysis owing to its excellent air pollution control and its ability to fully disintegrate harmful pollutants [4–7]. Since Fujishama and Honda discovered that water could be photo-catalytically split into hydrogen adsorption on a TiO_2 electrode, enormous efforts have been devoted to the research on TiO_2 material and considered a model system for studying small molecules [8].

Recently, it has been shown that photocatalytic H_2S splitting on TiO_2 surfaces is an eco-friendly way to eliminate H_2S [9–12], which can lead to clean energy H_2 [13–15] and realize sulfur recovery [16]. For instance, enormous work has been done concerning the H_2S interaction study with rutile and anatase surfaces which is important for H_2S photo-splitting and prevents its emission into the atmosphere. A density functional theory (DFT) method has already been extensively used to provide qualitative and quantitative insights into the structure of active surfaces and surface reactions. Within this theory, the approximations used have been shown to provide an excellent balance between computational accuracy and cost which makes it ideal to understand the physics behind many materials. Huang and co-works [17] studied the adsorption and reaction of H_2S on TiO_2 rutile (110) and anatase (101) surfaces using DFT (GGA + PW91) and a periodic supercell under the VASP code. This showed that both molecular and dissociated adsorption was observed. Fang Wang *et al.* [18] present different results for H_2S adsorption/dissociation on perfect TiO_2 (110) surface using DFT + U with (GGA + PW91) and (LDA + PW91) as implemented in CASTEP code. They investigate the oxygen role vacancies in dissociating H_2S on the Rutile (110) surface. It was found that H_2S is dissociated directly into HS/H over vacancy $V(O_2)$ and adsorbs molecularly over Ti_{5c} site on the perfect surface. Among the different TiO_2 polymorphs, Rutile TiO_2 (110) has been one of the most widely studied surfaces in surface science [19, 20].

Although many theoretical investigations on H_2S adsorption and dissociation on TiO_2 Rutile (110) surface have been conducted, there is still a need for more investigations to determine and predict possible scenarii of this process using different DFT approaches. In this work, we investigate the adsorption and dissociation of H_2S on the TiO_2 rutile (110) surface using DFT + U calculation and the general gradient approximation (GGA) with the Perdew-Burke-Ernzerhof (PBE) functional under VASP code including adsorption energy, geometrical structural, the density of states curves, bandgap and work function changes with charge transfer. The results analyses have shown the relation between adsorption energy and distance of H_2S-TiO_2 surface. By including PBE + D2 interactions, the adsorption energies of the most stable configuration were increased, implying the dispersion energy dominant effect. This work is dedicated to gaining important insight into the adsorption of harmful H_2S molecules using DFT (PBE + U/D2) approach and its effect on the Photocatalysis properties.

2. COMPUTATIONAL DETAILS

All calculations were performed by density functional theory (DFT) as implemented in Vienna Ab-initio Simulation Package (VASP) [21–22]. The exchange-correlation energy was calculated using the Perdew-Burke-Ernzerhof (PBE) functional

within the general gradient approximation (GGA) [24]. The projected augmented wave (PAW) method [23] was employed to treat valence-core interactions with 12, 6, 6, and 1 valence electrons for Ti, O, S, and H, respectively. The kinetic energy cut-off for the plane-wave basis was set to 500 (eV). Additionally, for PBE + U calculations, the on-site Coulomb repulsion parameter U was decided so as to reproduce a correct band-gap value of bulk rutile TiO_2 (3.02 eV), which was found to be 9.0 (eV) for the Ti 3d orbital as shown in Fig. 1 and as consistent with previous literature [18, 25, 31].

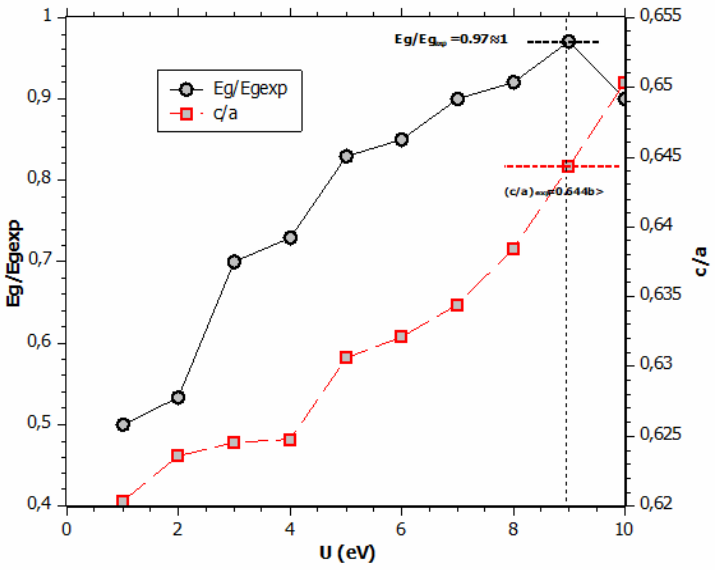

Fig. 1 – Electronic bandgap for bulk rutile TiO_2 plotted against U-values in comparison with the experimental value.

In this work (3 × 2 × 1) rutile TiO_2 (110) surface supercell ($Ti_{36}O_{72}$) was simulated by using a periodic slab method with a thickness of three O-Ti-O layers and about 14 (Å) vacuum regions to avoid any interactions between the adjacent surface. During the structure optimization, the adsorbate and the two top O-Ti-O surface layers were fully relaxed in all directions, while the bottom O-Ti-O layer was fixed to mimic the bulk structure. The molecule was adsorbed only on one side of the slab. The convergence criterion for the electronic self-consistent loop was set to 10^{-5} eV. The calculated lattice parameters of the rutile TiO_2 unit cell are $a = b = 4.6916$ Å and $c = 3.065$ Å, which are in reasonable agreement with the experimental value of $a = b = 4.5938$ Å and $c = 2.9586$ Å [32]. All the calculations were carried out using the Brillouin zone sampled with a (5 × 5 × 1) Monkhorst-Pack mesh k-point grid [33]. Spin polarization and dipole correction were applied for all calculations. For this purpose, Grimme's DFT-D2 [34] method was employed in this study to consider

the effect of long-range van der Waals interaction. The adsorption energies E_{ad} was calculated using the following equation:

$$E_{ad} = E_{mol/surf} - (E_{mol} + E_{surf}) \quad (1)$$

where $E_{mol/surf}$, E_{mol}, and E_{surf} are the total energies calculated for the slab with adsorbate, the clean stoichiometric slab, and the adsorbate in the gas phase, respectively. According to Eq. 1, a negative value of ΔE_{ad} indicates an exothermic adsorption system. The adsorption energies are used to evaluate the most favourable adsorption sites. Charge transfer between the adsorbate and the surface was analysed using the Bader atomic charge method [35] and defined as the difference between the net charge of H_2S before and after adsorption.

3. RESULTS AND DISCUSSION

3.1. OPTIMIZED STRUCTURES

Full optimizations of the isolated H_2S molecule and pure rutile TiO_2 surface were initially performed using the identical supercell of 9.23 × 13.29 × 24.24 $Å^3$ to confirm the accuracy of the calculation methods. The predicted H-S bond length and H-S-H bond angle of H_2S molecule are 1.35 Å and 91.3°, respectively, which agrees with experimental values of 1.328 Å and 92.2° [37, 38]. Figure 2 depicts the atomic structure of the clean rutile TiO_2 (110) (3 × 2 × 1) surface, which is terminated by bridging oxygen atoms O_{2c} and is composed of fivefold and sixfold coordinated Ti atoms, as well as threefold coordinated oxygen. We compare the calculated atomic displacements due to surface relaxations in the perpendicular direction to the surface with experimental and theoretical work summarized in Table 1. The positive and negative values represent the atomic displacement along the *z*-axis. Table 1 shows that the atomic relaxations agree well with experimental and previous studies, indicate that our computation model is reliable. The predicted surface energy of the relaxed surface converges to 0.51 J/m^2, which is comparable to the values of 0.47 and 0.35 J/m^2 found by Keijna *et al.* [39] and Lazzeri *et al.* [39] with different *n*-layers. Surface formation is well known to result in a decrease in the bandgap width of a particular material [41, 42]. The calculated band-gap width for pure rutile (110) surface is 2.6 eV (Fig. 3), which is less than the equivalent value for the bulk 2.9 eV (3.02 eV experimental value) [32]. The shift in energies of the O-2p and Ti-3d states for the fixed O and Ti atoms is primarily responsible for the bandgap narrowing. At higher energies, the 2p states of O atoms form the valence band (VB) maximum. Ti-3d states dominate the bottom of the conduction band (CB) and slightly move the CB minimum downward. In the upper VB and CB areas, there is significant hybridization between the O-2p atomic orbitals and the Ti-3d.

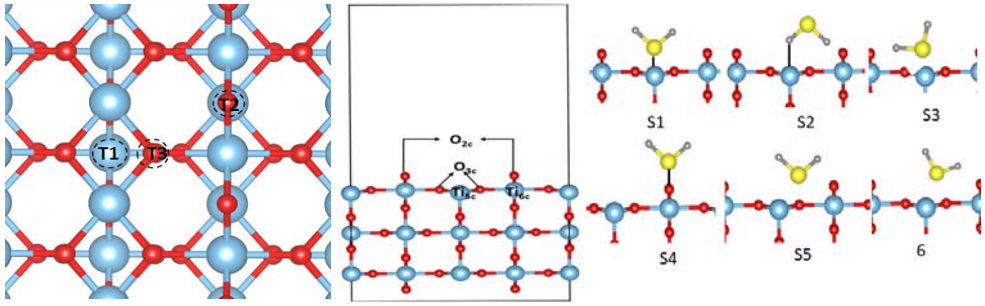

(a) (b) (c)

Fig. 2 – The optimized structures of: a) top; b) side view of TiO_2 (110) (3 × 2) surface with adsorption position of H_2S molecule are labeled by T1, T2, and T3 respectively; c) initial stats structure of three kinds of H_2S adsorption.

Table 1

The predicted atom relaxation of the perfect TiO_2 (110) surface along the *z*-axis together with experimental data

Atoms	SXRD [40]	This work	Ref. [18]
O2c	–0.27±0.08	–0.005	–0.007
O3c	0.05±0.05	0.166	0.152
Osub	0.05±0.08	–0.089	–0.002
Ti5c	–0.16±0.05	–0.127	–0.158
Ti6c	0.12±0.05	0.112	0.193

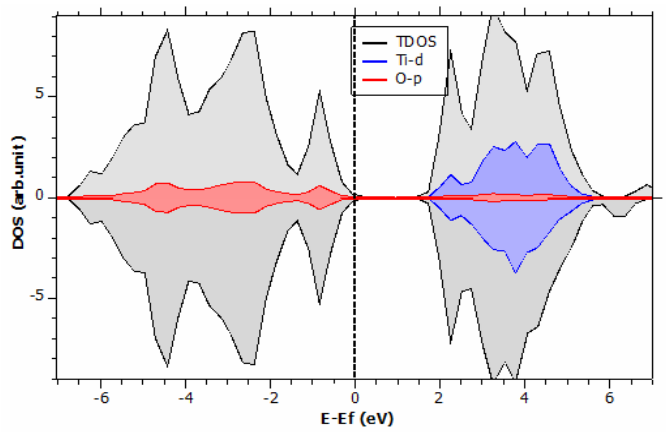

R-TiO_2 (110) clean surface

Fig. 3 – Total and partial DOS of TiO_2 rutile (110) surface.

It is a well-known fact that surface creation is accompanied by a reduction in the bandgap width of a given material [41, 42]. The computed band-gap width is equal to 2.6 eV for pure rutile (110) surface (Fig. 3), which is less than the

corresponding value for the bulk 2.9 eV (3.02 eV experimental value) [32]. The origin of the band-gap narrowing is mainly due to the change in energies of the O-2p and Ti-3d states for the fixed O and Ti atoms. The 2p states of O atoms are found at higher energies forming the valence band (VB) maximum. The Ti-3d states dominate the bottom of the conduction band (CB) and shift the CB minimum slightly downward. A considerable hybridization occurs between the O-2p atomic orbitals and the Ti-3d in the upper VB, as well as in the CB regions.

3.2. ADSORPTION STRUCTURE AND ENERGY

H_2S molecule can interact with TiO_2 (110) surface in several different ways by using its H atoms and S lone pair electrons. To understand the adsorption mechanism more comprehensively, we consider three adsorption sites T1-T3 of Fig. 2a, and there are three initial adsorption states of H_2S, as shown in Fig. 2c. To analyse the adsorption/interaction mechanism of the different adsorption positions and different initial states of H_2S molecule, which can be seen in Table 2. The most stable configurations of the adsorption systems are shown in Fig. 4. One can observe clearly that H_2S prefers to adsorb disociatively over rutile TiO_2 (110) surface. Table 2 summarizes the adsorption energy, the bond length of the newly formed Ti-S and H-O bonds, S-H bonds of the adsorbed H_2S molecule upon the adsorption process.

Table 2

Adsorption energy, calculated new bond length for the different configurations

	E_{ad} (eV)		S-Ti_{5c} (Å)	H-S (A°)	H-O_{2c} (Å)
	PBE + U	PBE + U + D2			
T1-S1	–1.1524	–1.5230	2.717	1.35	–
T1-S2	unstable	–	–	–	–
T1-S3	–1.7500	–2.3201	2.460	1.35	1.00
T2-S4	–1.2542	–1.6575	2.470		–
T2-S5	–1.7570	–2.3210	2.459	1.35	0.99
T3-S6	–1.7560	–2.3203	2.461	1.35	1.00
Ref. [19]	–1.71 –2.16	–1.03 –1.44	2.60 2.43	1.35	1.54 1.07

After achieving systems structure relaxation, one can obtain the optimal geometry; the under-coordinated titanium sites were strongly favoured during the adsorption process. The S atoms from the H_2S molecule bind preferentially to the fivefold coordinated titanium (Ti_{5c}) atom of the TiO_2 surface. The computed Ti_{5c}-S bond lengths are 2.717, 2.460, 2.470, 2.459, and 2.461 Å for S1, S3, S4, S5, and S6 configurations, respectively. After adsorption, the surface Ti-O bond and H-S bonds of the adsorbed molecule are changed due to the formation of a new bond S-Ti and the electronic density moves from this bond to the newly formed S-Ti_{5c}

bond between the molecule and surface. The surface atoms of the rutile TiO_2 (110) rearrange themselves due to the adsorption process, where Ti_{5c}-O_{3c} and Ti_{6c}-O_{2c} bond length tends to change around ± (0.01/0.02) Å and + 0.1 Å, respectively. The bond angle O_{3c}-Ti_{5c}-O_{3c} and O_{2c}-Ti_{6c}-O_{2c} has been changed by about + 1.14/2.8° and –5°, respectively (a positive value means a stretching, while a negative value means a shrinking of the bond length and bond angle).

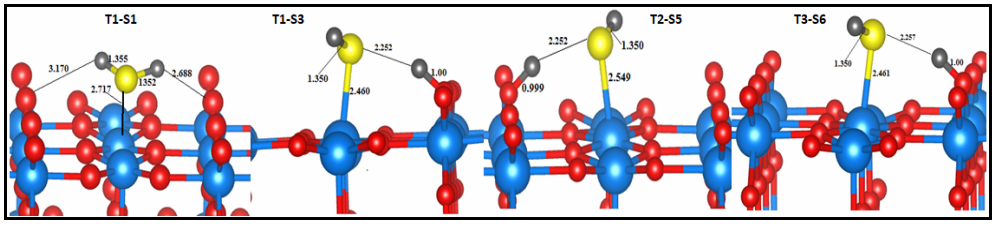

Fig. 4 – (Color online) Molecular and dissociated adsorption configurations of H_2S on rutile TiO_2 (110) surface. The blue, red, yellow, and gris represent titanium, oxygen, sulphur, and hydrogen respectively.

For the molecular adsorption configuration (T1-S1), the bond length for the adsorbed H_2S molecule does not change too much compared to its free states, changes in bond length do not exceed 0.002 ± 0.001 Å and 11° for the HSH angle. For dissociation adsorption configuration T1-S3, T1-S3, T2-S5 and T3-S6, the H_2S is dissociated to HS and H, where HS is adsorbed on Ti_{5c} with S-Ti_{5c} bond lengths of 2.460, 2.459, and 2.461 Å. The H-S bond length at HS changes about 0.002 ± 0.001 Å than that in the gas phase of H_2S, due to the S-Ti bond formation. The dissociated H from H_2S is adsorbed on an O_{2c} atom nearby with the H-O bond length of 1.00 Å. Where we can observe clearly that Ti_{5c} and Ti_{6c} participating in the adsorption process are displaced outward about 0.26 and 0.16 Å respectively due to the Ti_{5c}-S and O_{2c}-H bonds formation.

Adsorption energy analysis was conducted in this work to fully investigate the H_2S adsorption on the considered surface. Table 2 summarizes the adsorption energy calculated based on different sites. We observed that all the adsorption energies (E_{ads}) are negative, suggesting that all the adsorption processes can take place naturally. The adsorption energy of dissociated configurations T1-S3, T2-S5 and T3-S6 are higher (more negative) and very close, the T2-S5 is the most stable configuration with an adsorption energy of –1.7570 eV corresponding to higher CPU time and the short bond length (S-Ti_{5c}). The lowest adsorption energy is found for the molecular adsorption configuration T1-S1 (–1.1524 eV). The adsorption energy is slightly changed by considering the PBE + D2 interaction. For all configurations, the fivefold coordinated titanium atoms in the TiO_2 act as the binding sites and the H_2S prefers to interact with Ti_{5c} through its lone-pair electrons, similar to the previous studies reported by Huang *et al.* [18]. A comparison between the adsorption energy obtained by theoretical studies based on different approaches GGA + PBE, GGA + PW91 under VASP [17], and LDA + PW91 under CASTEP [18] is shown

in Fig. 5. The difference in adsorption energy between the presented results and those in Ref. [17, 18] may be caused principally to the used method (LDA/GGA with PBE/PW91) with or without considering the on-site coulomb U parameters and PBE + D2 interactions inside and the software used for DFT calculation (VASP/CASTEP). The relation between the molecule-surface distance d(S-Ti_{5c}) and the adsorption energy for the different configurations is shown in Fig. 5.

Table 3

Bader charge distribution analysis of H_2S

System	Species	Charge	Total
Free H_2S	S H1 H1	+ 2.3695 –1.1862 –1.1833	0
T1-S1	S H1 H1	2.47 –1.18 –1.17	–0.13
T1-S3	S H1 H1	0.743 –1.23 1.00	–0.51
T2-S4	S H1 H1	2.66 –1.15 –1.16	–0.35
T2-S5	S H1 H1	0.66 –1.20 1.10	–0.56
T3-S6	S H1 H1	0.75 –1.18 1.12	–0.69

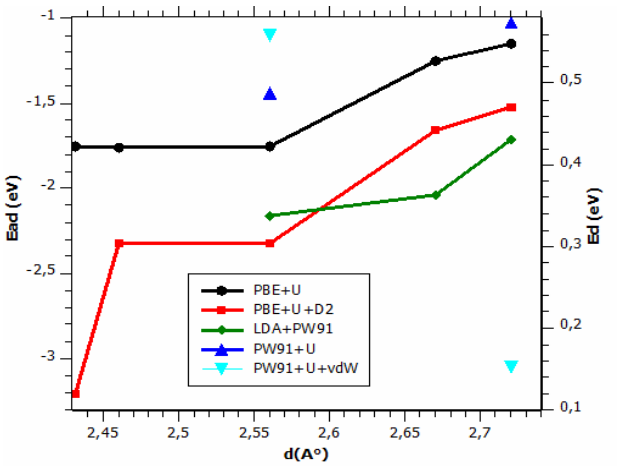

Fig. 5 – Adsorption energy (E_{ad}) against molecule-surface distance d(Ti-S) computed by DFT (+ U/ + vdW) in comparison to Ref. [18] (LDA + PW91) and Ref. [19] (LDA + PW91 + U/ GGA + PW91 + U + vdW).

3.3. ELECTRONIC STRUCTURE AND CHARGE TRANSFER

The total density of state and projected density of state are used to analyse the bandgap changes with a smearing factor of 0.2 eV. The interfacial bonding interactions were further investigated by TDOS and PDOS as shown in Fig. 6. It is interesting to note that a spin-up and spin-down peak appears at the same energy level and results in the almost symmetrical state which is composed of Ti-3d, O-2p, and S-2p states, this is due to the covalent Ti-S bond formation. In comparison with the perfect surface (Fig. 3), the results indicate that the interaction between the adsorbate and the surface has changed the electronic structure of the surface. Figure 6 shows that the upper valence band is dominantly composed of O-2p states, with a small contribution of Ti-3d and S-2p states. The hybridization of S-2p and Ti-3d, with the contribution of O-2p states, could promote charge transfer and enhance interfacial interactions. The conduction band is constituted mostly of Ti_{3d} and a small amount of S_{2p} states. The H_2S molecule adsorption on the rutile TiO_2 (110) surface showed interesting variation in the gap energy compared with a clean surface as reported in Table 4. The band gaps are reduced by about 0.8, 1.0, 0.9, and 0.7 eV for S1, S3, S5, and S6 configurations, respectively which can enhance the TiO_2 photocatalytic properties. The changes in Fermi energy are listed in Table 3. It is noteworthy to say that the change in bandgap leads to variations in conductivity that can be used to design a sensor. The connection between conductivity and energy bandgap can be described by Eq. 2:

$$\sigma \propto \exp(-E_g/kT). \tag{2}$$

Here, σ is the electric conductivity, and k denotes the Boltzmann constant. A small decrease in the bandgap results in significantly higher electrical conductivity. The TiO_2 rutile (110) surface bandgap is decreased by 0.8 (3%), 1.0 (46%), 0.9 (37%) and 0.7 (27%) upon interaction with H_2S molecules. Hence, this surface can be considered as a selective sensor for H_2S molecules.

To analyse the detailed features of charge transfer upon H_2S adsorption on the TiO_2 (110) surface, we have applied the Bader charge analysis technique to the different configurations and the results were listed in Table 3. The charge difference for the particle after and before adsorption was calculated using the following equation:

$$\Delta\rho = \rho_{i\ (in\ complexe)} - \rho_{i\ (in\ vacuum)}, \tag{3}$$

where ρ_i is the Bader charge value of the TiO_2 surface or H_2S molecule. $\Delta\rho$ is a measure of the extent of charge shifted to, or, from the studied surface from, or, to the H_2S molecule. For the T1-S3, T2-S(4-5) and T3-S6 structures, H_2S adsorption provides a charge transfer of about 0.51, 0.35, 0.56 , 0.69e, respectively, from surface to molecule, in comparison to 0.13 e for the T1-S1, suggesting that H_2S

acts as an electron acceptor. This leads to changes in the system conductivity, which would be an efficient property to help in the development of TiO_2-based sensors and remover devices for H_2S. The charge transfer magnitude seems to be correlated with the adsorption energy.

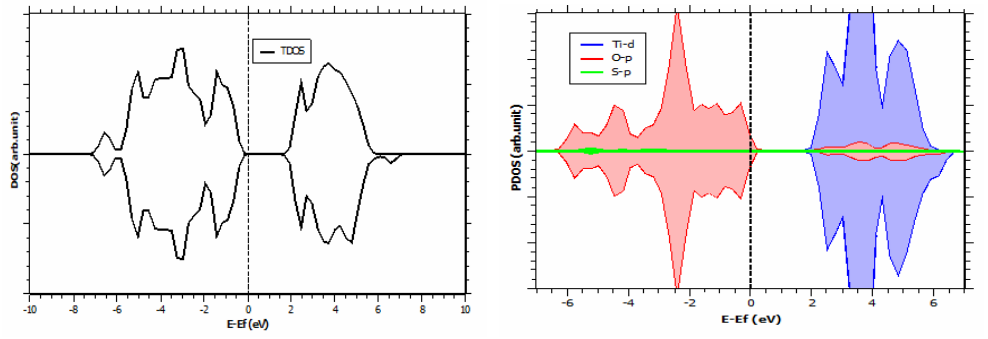

T1-S1

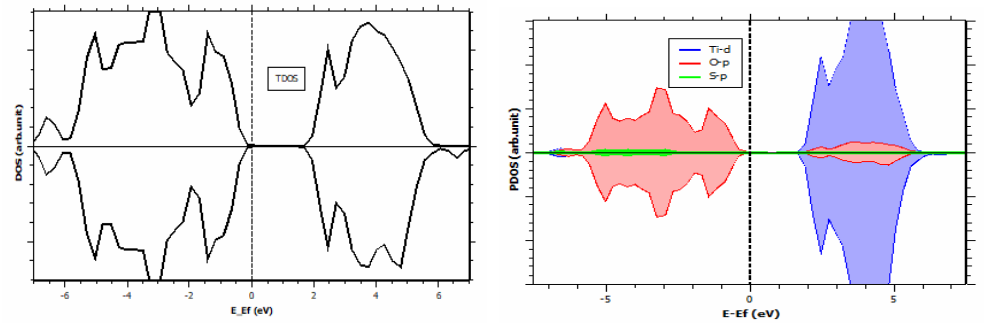

T1-S3

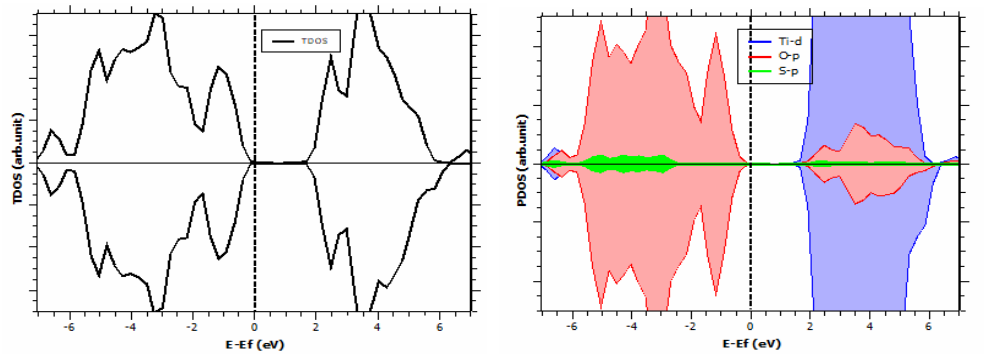

T2-S3

Fig. 6 – DOS and PDOS of the molecular T1-S1 and dissociated T1-S3 and T2-S3 adsorption configurations relative to Fermi level.

Table 4

Bandgap, Fermi energies, work function (WF), and its variation (ΔE_g and ΔWF) upon adsorption of H_2S at the rutileTiO_2 (110) surface

Configuration	E_g (eV)	WF (eV)	ΔE_g (%)	ΔWF (eV)
r-TiO_2 (110) surface	2.6	7.55	–	–
T1-S1	1.81	6.89	30	0.66
T1-S3	1.4	6.07	46	1.48
T1-S4	1.26	6.57	50	0.98
T2-S5	1.36	5.91	47	1.64
T2-S6	1.9	6.08	27	1.47

3.4. CHANGE OF WORK FUNCTION INDUCED BY ADSORPTION

The work function of a semiconductor is the lowest energy required by electrons at the bottom of the semiconductor to escape outside, and it can be defined as the difference between the potential in the middle of the vacuum layer and the fermi energy. The work functions (WF) have also been calculated to provide more information on these surface features. The work function is a fundamental characteristic of the solid surface that provides additional information on the electrical properties. Table 4 shows the WF values computed by DFT + U for TiO_2 (110) surface and the various configurations T1-3 (S1-6). For contrast, the computed work function of TiO_2 (110) surface is 7.55 eV, which agrees well with the theoretical values of 7.29 eV with $U = 10$ eV and 7.46 eV with $U = 0$ eV in Ref. [43]. The surface work function will be affected (reduced) by the adsorption of the H_2S molecule on the TiO_2 (110) surface. This is dependent on the adsorption site and charge transfer at the surface/molecule interface.

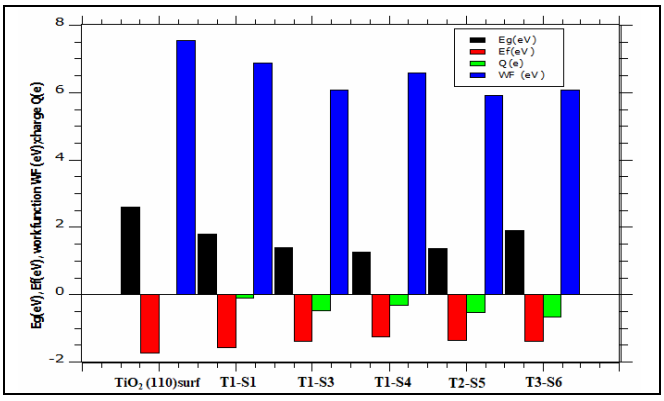

Fig. 7 – Variation of the work function, Fermi energy (E_f) and charge transfer of different structure.

It is found in the following order: TiO_2 (110) > S1 >S4 > S6 > S3 > S5. Furthermore, changes in the surface structure and the difference in electronegativity

of the S atom relative to H_2S and the Ti/O atoms of the TiO_2 surface led to the production of surface dipoles, which can reduce the WF. In Fig. 7, we depicted the work function, Fermi energy, and charge transfer for various structures. The work function decreased by 0.66 eV for the S1 structure and 1.48 eV, 0.98 eV, 1.64 eV, and 1.47 eV for the S3, S4, S5, and S6 structures, respectively. For comparison, a similar decrease was found for the water on the perfect surface about 1.1 eV–1.2 eV [44] and reduced surface 0.6 eV–0.9 eV [45].

4. CONCLUSION

This work focuses on the DFT + U computations study to investigate TiO_2 rutile (110) surface properties within the interaction with H_2S harmful gas. Different approaches based on generalized gradient approximation (GGA) with PBE + U and PBE + D2 under VASP code are successfully performed compared to the theoretical results. The adsorption energy, work function, and bandgap of H_2S molecule on rutile TiO_2 (110) surface with different H_2S-TiO_2 distances have been investigated. It has been found that for the different configurations, the H_2S prefers to adsorb at the surface Ti_{5c} site the most energetically suitable, letting the H atom bonded to another O_{2c} site. By including the van der Waals interaction (D2), the adsorption energy was increased. The Ti_{5c}-S and O_{2c}-H newly bonds formation confirms the Ti_{5c} and Ti_{6c} displacement outward about 0.26 and 0.16 Å. The adsorption energy is exactly correlated to the charge transfer magnitude. The electron transfer between the molecule and surface is calculated representing that the H_2S molecule acts as a charge acceptor. The PDOS plots show considerable overlaps between the contacting atoms, implying the formation of new chemical bonds. The change in the work function caused by the adsorption of H_2S on the surface relates to the adsorption site and charge transfer. The minimum work function is found for the dissociated adsorption configuration. The improved TiO_2 photocatalytic properties contribute to the energy gap shift to lower energies which increases the sensors' performance in H_2S gas detection.

REFERENCES

1. A. Fujishima, T.N. Rao, D.A. Tryk, J. Photochem. Photobiol. C. **1**, 1–21 (2000).
2. A. L. Linsebigler, G. Q. Lu, J. T. Yates, Chem. Rev. **95**, 735 (1995).
3. A. Fujishima, K. Honda, Nature **238**, 37–38 (1972).
4. V. V. Ursaki, S. Lehmann, V. V. Zalamai, V. Morari, K. Nielsch, I. M. Tiginyanu, E. V. Monaico, Romanian Journal of Physics **68**, 601 (2023).
5. H. Ibrahim, H. Lasa, Appl. Catal. B, Environ. **38**, 201–213 (2002).
6. I. Sopyan, M.watanabe, S. Murasawa, K. Hachimoto, A. Fujishima, Chem. Lett. **1**, 69–70 (1996).
7. A. Mills, S.Le.Hunte, J. Photoch. Photobio. A. **108**, 1–35 (1997).
8. A. Fujishima, X. Zhang, C.R. Chimie. **9**, 750–760, 2006.
9. V. Purcar, V. Rădiţoiu, F. M. Raduly, A. Rădiţoiu, S. Căprărescu, A. N. Frone, C. Nicolae, Romanian Journal of Physics **68**, 604 (2023).

10. S.B. Rasmussen, R. Portela, S. Suárez, J.M. Coronado, M.-L. Rojas-Cervantes, P. Avila, B. Sánchez, Ind. Eng. Chem. Res. **49**, 6685–6690 (2010).
11. R. Portela, S. Suárez, S.B. Rasmussen, N. Arconada, Y. Castro, A. Durán, P. Ávila, J.M. Coronado, B. Sánchez, Catal. Today **151**, 64–70 (2010).
12. S. Yu, Y. Zhou, *Photochemical decomposition of hydrogen sulfide*, L.E. Norena, J.-A. Wang (Eds.), InTech Press, Croatia, pp. 269–293, 2016.
13. G. Ma, H. Yan, J. Shi, X. Zong, Z. Lei, C. Li, J. Catal. **260**, 134–140 (2008).
14. N.S. Chaudhari, S.S. Warule, S.A. Dhanmane, M.V. Kulkarni, M. Valant, B.B. Kale, Nanoscale **5**, 9383 (2013).
15. A.P. Bhirud, S.D.Sathaye, R.P.Waichal, J.D.Ambekar, C.J.Park, B.B. Kale, Nanoscale **7**, 5023–5034 (2015).
16. K.V. Bineesh, D.-K. Kim, H.-J. Cho, D.-W. Park, J. Ind. Eng. Chem. **16**, 593–597 (2010).
17. W. F. Huang, H. T. Chen, M. C. Lin, J. Phys. Chem. C. **113**, 20411–20420 (2009).
18. F. Wang, S. Wei, Z. Zhang, G. R. Patzke, Y. Zhou, Phys. Chem. Chem. Phys. **18**, 6706–6712 (2016).
19. U. Diebold, *The surface science of titanium dioxide*, Surf. Sci. Rep. **48**, 53–229 (2003).
20. C.L. Pang, R. Lindsay, G. Thornton, Chem. Soc. Rev. **37**, 2328–2353 (2008).
21. G. Kresse, J.Hafner, Phys. Rev. B. **47**, 558–561 (1993).
22. G. Kresse, J. Furthmuller, Comput. Mater. Sci. **6**, 15–50 (1996).
23. G. Kresse, D. Joubert, Phy. Rev. B. **59**, 1758–1775 (1999).
24. J. P. Perdew, K. Burk, M. Ernzerhof, Phy. Rev. Lett. **77**, 3865–3868 (1996).
25. Y. Wang, D. J. Doren, Solid-State Commun. **136**, 142–146 (2005).
26. S. L. Dudarev, G.A. Botton, S.Y. Savrasov, C.J. Humphreys, A.P. Sutton, Phys. Rev. B. **57**, 1505–1509 (1998).
27. V. I. Anisimov, F.Aryasetiawan, A. I. Lichtenstein, J. Phys. Condens. Matter. **9**, 767–808 (1997).
28. M. Nolan, S.Grigoleit, D.C. Sayle, S.C.Parker, G. W. Waston, Surf. Sci. **576**, 217–229 (2005).
29. X.G. Ma, Y. Wu, Y.H. Lu, J. Xu, Y.J. Wang, Y.F. Zhu, J. Phys. Chem. C. **115**, 16963–16969 (2011).
30. M. Sieberer, J. Redinger, P. Mohn, Phys. Rev. B. **75**, 035203 (2007).
31. R. Coquet, D.J. Willock, Phys. Chem. Chem. Phys. **7**, 3819–28 (2005).
32. A. Stashans and Y. Bravo, Mod. Phys. Lett. B **27**, 1350113 (2013).
33. H.J. Monkhorst, J.D. Pack, Phys. Rev. B **13**, 5188–5192 (1976).
34. S. Grimme, J. Comput. Chem. **27** (15), 1787–179 (2006).
35. G. Henkelman, A. Arnaldsson, H. Jónsson, Comput. Mater. Sci. **36**, 254 – 360 (2006).
36. E.J. Albenze, A. Shamsi, Surf. Sci. **600**, 3202–3216 (2006).
37. R.C. Shiell, X.K. Hu, Q. J. Hu, J.W. Hepburn, J. Phys. Chem. A **104**, 4339–4342 (2000).
38. A. Keijna, T. Pabisiak, S. W. Gao, J. Phys. Condens. Matter. **18**, 4207–4217 (2006).
39. M. Lazzeri, A. Vitttadini, A. Selloni, Phys. Rev. B **65**, 155409 (2002).
40. G. Charlton, P.B. Howes, C.L. Nicklin, P. Steadman, J.S.G. Taylor, C.A. Muryn, S.P. Harte, J. Mercer, R. McGrath, D. Norman, Phys. Rev. Lett. **78**, 495–498 (1997).
41. N. Martsinovich, D. Jones, A. Troisi, J. Phys. Chem. C **114**, 22659 (2010).
42. A. Stashans *et al.*, Phil. Mag. B **81**, 1977 (2001).
43. E. German, R. Faccio, A. W. Mombru, Applied Surface Science **428**, 118–123 (2018).
44. K. Onda, B. Li, H. Petek, Phys. Rev. B: Condens. Matter. Phys. **70**, 0454151–0454151 (2004).
45. J. N. Muir, Y. Choi, H. Idriss., Phys. Chem. Chem. Phys. **14**, 11910–11919 (2012).